Author Manuscript

Author Manuscript

Author Manuscript

Author Manuscript

HHS Public Access

Author manuscript

ACS Nano. Author manuscript; available in PMC 2019 January 23.

Published in final edited form as:

ACS Nano. 2018 January 23; 12(1): 109–116. doi:10.1021/acsnano.7b07720.

Nanoparticle Functionalization with Platelet Membrane Enables Multi-Factored Biological Targeting and Detection of Atherosclerosis

Xiaoli Wei, **Man Ying**, **Diana Dehaini**, **Yuanyuan Su**, **Ashley V. Kroll**, **Jiarong Zhou**, **Weiwei Gao**, **Ronnie H. Fang**, **Shu Chien**, and **Liangfang Zhang***

Department of NanoEngineering, Department of Bioengineering, and Moores Cancer Center, University of California San Diego, La Jolla, CA 92093, U.S.A

Abstract

Cardiovascular disease represents one of the major causes of death across the global population. Atherosclerosis, one of its most common drivers, is characterized by the gradual build-up of arterial plaque over time, which can ultimately lead to life-threatening conditions. Given the impact of the disease on public health, there is a great need for effective and noninvasive imaging modalities that can provide valuable information on its biological underpinnings during development. Here, we leverage the role of platelets in atherogenesis to design nanocarriers capable of targeting multiple biological elements relevant to plaque development. Biomimetic nanoparticles are prepared by coating platelet membrane around a synthetic nanoparticulate core, the product of which is capable of interacting with activated endothelium, foam cells, and collagen. The effects are shown to be exclusive to platelet membrane-coated nanoparticles. These biomimetic nanocarriers are not only capable of efficiently localizing to well-developed atherosclerotic plaque, but can also target subclinical regions of arteries susceptible to plaque formation. Using a commonly employed magnetic resonance imaging contrast agent, live detection is demonstrated using an animal model of atherosclerosis. Ultimately, this strategy may be leveraged to better assess the development of atherosclerosis, offering additional information to help clinicians better manage the disease.

Graphical abstract

*Corresponding author, Tel: 858-246-0999, zhang@ucsd.edu.

ASSOCIATED CONTENT

The authors declare no competing financial interest.

Author Manuscript Author Manuscript Author Manuscript Author Manuscript

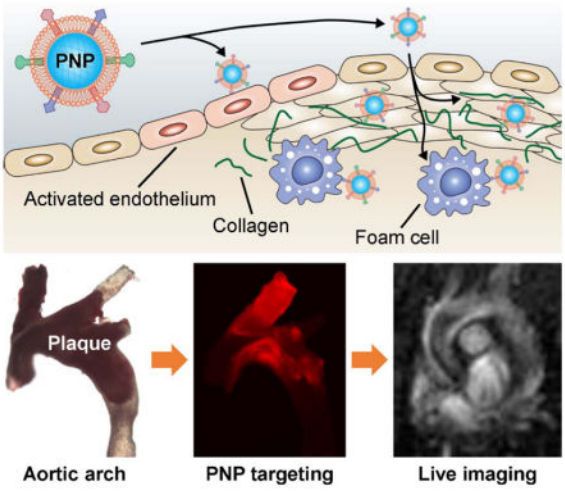

Keywords

cardiovascular disease; atherosclerosis; biomimetic nanoparticle; platelet; biointerfacing; MRI

Cardiovascular disease is highly prevalent in many parts of the world and, depending on the population being studied, can account for nearly half of all deaths.[1,2] Among its different forms, coronary artery disease and cerebrovascular disease are the most common. These diseases generally involve the process of atherosclerosis, which follows a well-studied progression that results in the gradual thickening of arterial walls over time.[3,4] The condition is initiated by dysfunction of the endothelial layer, which can lead to the accumulation of oxidized low-density lipoprotein (LDL) in the intimal layer and promote local inflammation.[5,6] This process eventually leads to the recruitment of monocytes, which traverse the endothelial layer and differentiate into macrophages.[7] As these white blood cells ingest the LDL particles, some eventually die and rupture, which potentiates a positive feedback loop that recruits even more immune cells to the area.[8,9] Over time, a lipid core will form while a collagen-rich fibrous cap develops, covering the growing atheroma and separating it from the arterial lumen.[10,11] As the atherosclerotic plaque continues to grow, it increasingly obstructs blood flow and can cause a variety of conditions that affect quality of life.[12] In many cases, the plaque can rupture, leading to a thrombotic event that often results in a heart attack or stroke, both of which can be fatal.[13,14] Despite its prevalence, it is generally accepted that most deaths resulting from atherosclerosis can be prevented with lifestyle modifications,[15] making effective detection and monitoring of plaque development of the utmost importance.[16]

A major challenge in addressing atherosclerosis as it develops is that patients are generally asymptomatic until the very late stages when significant vessel occlusion occurs, or until there is a traumatic event caused by plaque rupture.[17] Currently, there are various strategies that can be applied towards the imaging of atherosclerotic plaque in the clinic.[18–20] Non-invasive modalities such as coronary computed tomography angiography, nuclear perfusion imaging, and cardiac magnetic resonance perfusion imaging can be effective at providing

Author Manuscript Author Manuscript Author Manuscript Author Manuscript

physical information such as the degree of occlusion, or the presence of hard calcification. These techniques, however, are not adept at tracking the biological development of the disease, and plaque build-up generally must be fairly advanced for accurate visualization. More invasive techniques such as intravascular ultrasound, optical coherence tomography, and coronary angiography can achieve higher resolution and provide significantly more information on atherosclerotic plaques, including superficial features, vulnerability characteristics, and biological composition. A hurdle in their widespread use is that they can carry significant risks due to their invasive nature, making their application for general purpose monitoring over time impractical. As it stands, the development of a strategy for the imaging of atherosclerosis that is both facile to apply and can provide additional biological information regarding plaque development would be highly beneficial.

Platelets, which are generally responsible for maintaining hemostasis within the body, have been heavily implicated in atherogenesis at multiple stages of development.[21–24] It has become increasingly apparent that, even at the outset, there is significant crosstalk between platelets and inflamed endothelium.[25,26] They are also capable of binding to immune cells and recruiting them to sites of inflammation. Finally, their hemostatic properties necessitate that they bind strongly to exposed subendothelial matrices, particularly those rich in collagen, and it is their binding at sites of plaque rupture that can lead to the deadly thrombus formation commonly seen in the clinic.[27,28] Given the multitude of interactions in which platelets participate, we sought to directly leverage these biological affinities to design a naturally targeted nanoparticle-based imaging platform capable of effectively localizing to atherosclerotic sites (Figure 1a). This was done by directly coating cell membrane derived from platelets onto a synthetic nanocarrier,[29] and the resulting platelet membrane-coated nanoparticles (PNPs) demonstrated a marked ability to bind different components of atherosclerotic plaques *in vitro*. The specificity afforded by the platelet membrane was further confirmed *ex vivo* using aortic arch samples obtained from mice with established atherosclerosis. This translated to effective targeting *in vivo*, effectively localizing the nanoparticles and their payload to the plaque region. Finally, it was shown that, by incorporating an MRI imaging agent into the PNP formulation, it was possible to generate sufficient contrast to distinguish the presence of plaque during live imaging. With the multifactorial detection afforded by the platelet membrane functionalization, it is possible to probe for the development of atherosclerosis and interrogate potentially diseased tissue in a biologically relevant manner.

Results and Discussion

PNPs were fabricated by coating the membrane derived from platelets onto preformed poly(lactic-*co*-glycolic acid) (PLGA) cores loaded with a far-red fluorescent dye, which was used as a model payload to demonstrate the ability of the nanoparticles to target atherosclerotic plaque. Briefly, PLGA was mixed together with 1,1′-dioctadecyl-3,3,3′,3′-tetramethylindodicarbocyanine (DiD) in an organic phase, which was then precipitated into an aqueous phase to form DiD-loaded polymeric cores. Platelets were derived fresh from blood *via* differential centrifugation, and platelet membrane was prepared using a repeated free-thaw process. Then the DiD-loaded cores and the membrane were mixed together and sonicated, resulting in membrane-coated nanoparticles. Using dynamic light scattering, it

Author Manuscript Author Manuscript Author Manuscript Author Manuscript

was determined that the final product was slightly larger than the bare PLGA cores in size (Figure 1b), and the surface zeta potential of the PNPs approached that of the platelet membrane-derived vesicles (Figure 1c), both results being indicative of successful membrane coating. The platelet membrane coating also helped to enhance the colloidal stability of the PLGA cores, which are normally unstable and aggregate when subject to physiological salt concentrations (Figure 1d). Additionally, transmission electron microscopy of PNPs negatively stained with uranyl acetate revealed the characteristic core-shell structure of membrane-coated particles,[30–32] with a lipid membrane coating forming a ring around the nanoparticulate core; the observed sizes of the nanoparticles were consistent with the dynamic light scattering measurements (Figure 1e).

After confirming successful nanoparticle fabrication, we conducted *in vitro* evaluations to explore the binding potential of the PNPs to different elements that play a role in atherogenesis. First, the ability of the particles to bind foam cells, which are largely responsible for the deposition of lipid-rich material during plaque development,[33] was assessed. Mouse J774 macrophages were converted to foam cells by culturing them with oxidized LDL, and the cells were subsequently fixed and incubated either with PLGA nanoparticles functionalized with polyethylene glycol (denoted 'PEG-NPs'),[34] red blood cell membrane (denoted 'RBCNPs'), or platelet membrane (PNPs). It was observed both by flow cytometric analysis, as well as by fluorescent imaging, that PNPs much more readily bound to the foam cells (Figure 2a,b). Next, the binding of the particles to collagen, which is a major component of the fibrous cap that sits on top of the atheroma,[10,11] was evaluated. Assay plates were coated with type IV collagen and incubated with the different nanoparticle solutions. Again, the PNPs demonstrated significantly higher binding compared with both PEG-NPs and RBCNPs (Figure 2c). Further, this effect was specific to collagen, as uncoated wells showed similarly low levels of binding among all the nanoparticle samples. Finally, the ability of the particles to bind to activated endothelium, which plays a major role in initiating the process of atherosclerosis,[35] was tested. Human umbilical vein endothelial cells (HUVECs) were activated with tumor necrosis factor alpha (TNF-α) and incubated with the various types of nanoparticles. On the activated endothelial cells, PNPs interacted much more strongly than the other samples. This difference was significantly lessened on resting HUVECs that were not subject to activation (Figure 2d). Overall, these results clearly demonstrated that PNPs possess particularly strong affinity with multiple components important to the formation of atherosclerotic plaque.

Given the encouraging *in vitro* results, we sought to further verify the ability of PNPs to bind with formed plaque by employing a murine model of atherosclerosis. ApoE knockout (KO) mice, which naturally develop plaque over time,[36] were fed on a high-fat western diet, after which their aortic arches were excised and incubated *ex vivo* with different nanoparticle types. After incubating with PEG-NPs, RBCNPs, or PNPs, the vessels were washed and observed under fluorescence microscopy. Both the PEG-NP and RBCNP controls exhibited negligible signal, whereas the high amount of signal for the PNPs demonstrated significant binding across the entirety of the plaque area (Figure 3a). Using Oil Red O lipid staining, the presence of plaque was then visually verified for each artery sample. This enhanced binding effect was further confirmed on histological samples, in which the different types of nanoparticles were incubated with cross-sections from a plaque-containing artery. Again, the

Author Manuscript Author Manuscript Author Manuscript Author Manuscript

PNPs displayed significant signal throughout, including directly on the plaque area across the luminal face of the vessel (Figure 3b). To verify that this binding effect was specific to samples from atherosclerotic mice, the experiment was repeated using wild-type mice with healthy aortic arches. In this case, the PNPs had minimal binding to the luminal side of the vessel, with some binding along the edges where there was exposed subendothelium due to the incision that was made to flatten the tissue sample for imaging (Figure 3c,d).

In addition to observing nanoparticle binding to areas with overt plaque formation, we also explored asymptomatic regions of arteries from the ApoE KO mice fed with the high-fat western diet. To this end, a section further down the aortic arch proximal to where plaque usually develops was chosen. With enough time, these regions will also develop visible atherosclerotic plaque, indicating that the underlying biological processes of atherogenesis are most likely present despite lack of ready evidence. For the experiment, visual observation was used to confirm the lack of plaque on these arteries, and they were then incubated with the different nanoparticle samples to assess binding. As shown in Figure 3e, while PEG-NPs and RBCNPs again showed minimal binding across the face of the arteries, the PNPs in contrast displayed an appreciable amount of signal, albeit less than was observed for the corresponding sample in Figure 3a. Afterwards, Oil Red O staining was conducted to further verify that there was no plaque present. The ability of the PNPs to bind such regions that are susceptible to plaque formation indicate that the nanoparticles may have utility for early stage detection, taking advantage of the biological mechanisms of platelet binding to probe for precursor processes before actual plaque formation.

Following the *ex vivo* binding evaluation, we next explored the ability of the PNPs to target the same atherosclerotic regions *in vivo* using a live animal model. ApoE KO mice were fed a high-fat western diet, allowing for the development of plaque over time. Subsequently, solutions of either PEG-NPs, RBCNPs, or PNPs were intravenously administered *via* the tail vein. After 24 hours, the mice were euthanized and their aortic arches analyzed for the presence of fluorescent signal (Figure 4a,b). Oil Red O staining was again used to macroscopically confirm the presence of plaque for each artery sample. Consistent with the *ex vivo* results, the arteries of mice administered with PNPs displayed significant fluorescent signal, while the signal for the other particles was negligible. To confirm that this effect was exclusive to atherosclerotic sites, the same experiment was performed in wild-type mice, and this yielded arteries with virtually no signal for all nanoparticle types. These results suggest that the PNPs, with their natural platelet membrane coating, are well-equipped to navigate through circulation and preferentially distribute to diseased tissue over healthy tissue.

Histological sections were then taken to obtain a more detailed microscopic view of the *in vivo* PNP targeting to atherosclerotic and pre-atherosclerotic regions. In the first instance, we analyzed a tissue sample with significant plaque development that resulted in a high degree of vessel occlusion (Figure 4c). By studying the distribution of the far-red dye in the PNP formulation, it was confirmed that the nanoparticle signal could be found in significant amounts throughout the plaque region. Sections were then stained with separate antibodies to probe for various elements of atherosclerosis development. This included ICAM-1 for activated endothelial cells, CD68 for macrophages, as well as type IV collagen. Each of the three was found to be present, and they displayed high degrees of proximity or co-

Author Manuscript Author Manuscript Author Manuscript Author Manuscript

localization with the nanoparticle signal on the sections. In the second instance, a section was taken from a vessel with significantly less disease burden, and the region of endothelium proximal to the plaque was studied (Figure 4d). Upon staining for ICAM-1, it was confirmed that there was activated endothelial cells at this region. This signal co-localized well with PNP signal, confirming that the particles are capable of binding to regions that are plaque-free but susceptible to future development. In total, these *in vivo* targeting experiments further indicated the potential of the platelet membrane-coated formulation to bind with atherosclerotic sites at different stages of development, including pre-atherosclerotic regions with no visible sign of disease.

Finally, to confirm the utility of the PNP formulation for live imaging, PNPs were formulated with a clinically relevant magnetic resonance imaging (MRI) contrast agent. In this case, we chose to employ a lipid-chelated gadolinium (Gd), which could easily be inserted into the lipid bilayer of the platelet membrane. After using this Gd-inserted membrane to fabricate PNPs (denoted 'Gd-PNPs'), we confirmed that the resulting nanoparticles were similar to unmodified PNPs in terms of physicochemical characteristics, stability in PBS, and morphology (Figure 5a–c). The zeta potential of Gd-PNPs was slightly more negative than PNPs, likely due to the acidic nature of the lipid chelator. Additionally, the ability of the particles to provide MRI contrast in T_1-weighted mode was evaluated (Figure 5d). The Gd-PNPs provided a high amount of positive contrast and could easily be detected over background. The Gd-PNPs were then administered to live ApoE KO mice that had been fed a high-fat western diet (Figure 5e,f). Prior to Gd-PNP administration, the aortic arch area did not exhibit any appreciable contrast within the vasculature when observed under MRI. However, at 1 hour post-administration of the Gd-PNPs, positive contrast can clearly be seen, strongly suggesting that the particles had specifically targeted atherosclerotic plaque at the aortic arch within this short time window. To confirm that this region was indeed atherosclerotic, the mice were euthanized after imaging, and Oil Red O staining of the aortic arch showed that there was significant fatty plaque present. This study established that PNPs could be used to successfully target and deliver a sufficient quantity of contrast agent to provide observable contrast at the site of interest. It should be noted that previous studies have demonstrated PNPs to be absent of pro-thrombotic factors, alleviating concerns of aggregation or clot formation at the target site.[29] Additionally, nanoparticulate formulations employing chelated Gd have been shown to be well tolerated at high doses in nonhuman primates.[37]

Conclusions

We have demonstrated that, by employing platelet membrane as a functional coating for nanocarriers, it is possible to effectively target imaging payloads to sites of atherosclerosis. This strategy leverages the natural interaction of platelet membrane markers with multiple components present during atherogenesis, including activated endothelium, foam cells, and collagen. It was shown that the PNPs can not only bind to regions with significant plaque formation, but also to areas that are pre-atherosclerotic and prone to plaque formation. Beyond simply providing contrast, this strategy also provides information about the underlying biology of the targeted regions, which may eventually be used to give a more complete picture of disease development over time. While MRI imaging was used in the

Author Manuscript Author Manuscript Author Manuscript Author Manuscript

present work as a proof-of-concept modality, given the generalizability of the cell membrane-coating technology,[38–40] it can be envisioned that the strategy outlined here can be adapted towards a variety of imaging modalities. This may ultimately enable improvements in specificity that can aid in the prevention and management of cardiovascular diseases, significantly mitigating their impact on global health.

Materials and Methods

Preparation and characterization of platelet membrane-coated nanoparticles (PNPs)

PNPs were fabricated according to a previously reported method.[29] Whole blood from male ICR mice (Envigo) was collected *via* puncture of the submandibular vein using 10 mM ethylenediaminetetraacetic acid (EDTA; USB Corporation) as an anticoagulant. All animal experiments were performed in accordance with NIH guidelines and approved by the Institutional Animal Care and Use Committee (IACUC) of the University of California San Diego. The platelets were isolated by differential centrifugation and the membrane was derived using a repeated freeze-thaw process.[41] Poly(lactic-*co*-glycolic acid) (PLGA; carboxyl acid-terminated, 0.67 dL/g, 50:50 monomer ratio; LACTEL Absorbable Polymers) nanoparticles were prepared by nanoprecipitation. Briefly, PLGA dissolved in acetone was precipitated into distilled water and allowed to evaporate under vacuum. Fluorescently labeled nanoparticles were fabricated by incorporating 1,1′-dioctadecyl-3,3,3′,3′-tetramethylindodicarbocyanine, 4-chlorobenzenesulfonate salt (DiD; Biotium) with the PLGA at 0.1 wt% during the synthesis of the cores. The final PNPs were fabricated by coating platelet membrane onto the preformed PLGA cores at a membrane protein to polymer weight ratio of 1:1 by sonicating in a Fisher FS30D bath sonicator. Size and zeta potential were measured by dynamic light scattering using a Malvern ZEN 3600 Zetasizer. Nanoparticle stability was assessed by measuring size after adjusting nanoparticle solutions to 1′ phosphate buffered saline (PBS). To visualize nanoparticle structure, transmission electronic microscopy (TEM) was performed by depositing the particles onto a 400-mesh carbon-coated copper grid (Electron Microscopy Sciences) and staining with 1 wt% uranyl acetate (Electron Microscopy Sciences), followed by observation under a Zeiss Libra 120 PLUS EF-TEM transmission electron microscope.

In vitro foam cell binding

The J774 mouse macrophage cell line (TIB-67; American Type Culture Collection) was cultured and maintained in DMEM (Mediatech) supplemented with 10% FBS (Hyclone) and 1% penicillin–streptomycin (Gibco). For foam cell conversion, the J774 cells were cultured for 48 hours in the presence of 50 μg/mL oxidized low density lipoprotein (LDL) (Bio-Rad).[42] Oil Red O (Sigma Aldrich) staining was used to confirm the desired phenotype. Briefly, the cells were fixed in 10% phosphate buffered formalin (Fisher Scientific), rinsed in 60% isopropanol, stained with filtered Oil Red O solution, destained with 60% isopropanol, and finally washed with PBS. Under bright field observation, the cells appeared red in color, confirming successful conversion. For the binding studies, the converted cells were fixed in 10% formalin and subsequently incubated with DiD-loaded PNPs, RBCNPs, or PEG-NPs at a concentration of 0.2 mg/mL for 30 minutes. The cells were then washed three times with PBS to remove unbound nanoparticles. For imaging, the cells were mounted in

Author Manuscript Author Manuscript Author Manuscript Author Manuscript

VECTASHIELD Antifade mounting media with DAPI (Vector Laboratories) and observed under a Keyence BZ-9000 fluorescence microscope. For flow cytometry, the cells were detached and data was collected using a FACSCanto II flow cytometer (BD Biosciences). Data analysis was performed using Flowjo software.

Collagen binding

Collagen type IV (Sigma Aldrich) was dissolved in 0.25% acetic acid at a concentration of 0.5 mg/mL. Afterwards, 100 μL of the collagen solution was added into a 96-well plate and incubated overnight at 4 °C. For the binding study, collagen-coated or non-coated plates were first blocked with 50% calf serum (Hyclone) for 1 hour and then incubated with 100 μL of 1 mg/mL DiD-loaded nanoformulations in 25% calf serum. After 1 hour of incubation, the plates were washed with PBS containing 0.05% Tween 20 (National Diagnostics) three times. Retained nanoparticles were then dissolved with 100 μL of dimethyl sulfoxide and quantified for fluorescence using a TeCan Infinite M200 plate reader.

Activated endothelial cell binding

HUVECs; Cell Applications) were maintained in human endothelial cell growth medium (Cell Applications). Confluent cells were stimulated with 50 ng/mL of TNF-α (Gibco) for 24 hours. For the cell binding study, activated or non-activated HUVEC cells were fixed with 10% phosphate buffered formalin for 30 minutes and blocked with 20% calf serum for another 30 minutes, followed by incubation with 0.2 mg/mL DiD-loaded nanoformulations in 20% calf serum. After 30 minutes of incubation on ice, the cells were washed three times and collected by scraping for data collection using a FACSCanto II flow cytometer (BD Biosciences). Data analysis was performed using Flowjo software.

Ex vivo adherence to atherosclerotic plaque

ApoE KO mice (B6.129P2-Apoe^{tm1Unc}/J; Jackson Laboratory) mice were fed with a high-fat diet (42% fat; TD88137; Envigo) for 4 months to promote the development of atherosclerotic plaque in the aortic arch. Age-matched ApoE KO mice and wild-type C57BL/6NHsd mice (Envigo) were euthanized and immediately perfused with PBS. The aortic arches were dissected and cut in half by making a longitudinal incision. For the arteries from the ApoE KO mice, samples were taken from regions with and without atherosclerotic plaque. For the wild-type mice, samples were collected from the same region where plaque usually develops in the ApoE KO mice. All samples were fixed in 10% phosphate buffered formalin for 30 minutes, blocked with 50% of calf serum for 1 hour, and then incubated with 0.2 mg/mL DiD-loaded nanoformulations for 30 minutes. The samples were then washed with PBS containing 0.05% Tween 20 three times before examination under a Keyence BZ-9000 fluorescence microscope. Afterwards, the same samples were subject to Oil Red O staining as described above to help visualize the presence of atherosclerotic plaque. For histological analysis, artery samples were embedded in Tissue-Tek OCT compound (Sakura Finetek) and cryosectioned, followed by fixation, blocking, and nanoparticle incubation using the same procedure as the whole tissue samples. The sections were mounted with DAPI-containing mounting media before imaging.

Author Manuscript Author Manuscript Author Manuscript Author Manuscript

In vivo targeting to atherosclerotic plaque

ApoE KO mice fed with a high-fat diet for 4 months and age-matched wild-type mice were intravenously administered with 0.5 mg of the various DiD-loaded nanoparticles *via* the tail vein. The nanoparticle dosage was chosen based on previous studies using PNPs to target vascular injury.[29] After allowing the nanoparticles to distribute for 24 hours, the mice were euthanized and then perfused with PBS to remove unbound nanoparticles. The aortas were isolated for imaging using a Keyence BZ-9000 fluorescence microscope. Oil Red O staining was performed to confirm the formation of atherosclerotic plaque in the ApoE KO mice. Quantification of fluorescence intensity was carried out using ImageJ software. For histological analysis, aortas from PNP-administered ApoE KO mice were collected and embedded in OCT compound for cryosectioning. Sections were then fixed in 10% formalin for 30 minutes and blocked with 4% bovine serum albumin (Sigma Aldrich). For fluorescent imaging, sections were incubated with anti-mouse CD54 (YN1/1.7.4; Biolegend), anti-mouse CD68 (FA-11; Biolegend) or polyclonal anti-collagen IV (ab6586; Abcam) followed by an Alexa Fluor 555-conjugated secondary (Biolegend). After washing three times with PBS containing 0.05% Tween 20, the sections were mounted with DAPI-containing mounting medium. All images were taken using a Keyence BZ-9000 fluorescence microscope.

Live magnetic resonance imaging of atherosclerotic plaque

To prepare nanoparticles for magnetic resonance imaging (MRI), a lipid-chelated gadolinium (Gd), DTPA-bis(stearylamide) (Gd salt) (Gd-DTPA-BSA; Avanti Polar Lipids), was used. A stock solution of the Gd-DTPA-BSA was prepared at a concentration of 10 mg/mL in 1:1 chloroform/methanol. 50 μL of the solution was then deposited into a glass vial and allowed to evaporate. The resulting film was then hydrated with solution containing 2 mg (protein mass) of platelet membrane at 37 °C for 30 minutes. Gd-incorporated PNPs (Gd-PNPs) were fabricated by fusing the Gd-containing platelet membrane with preformed PLGA cores through a sonication process. The PNPs were purified by spinning down the unincorporated Gd-DTPA-BSA precipitate at 1,000 ×g for 5 minutes. The Gd-PNPs were characterized by DLS and TEM as described above.

In vivo MRI was performed on a 4.7 T MR Solutions MRS 4000 preclinical MRI. The animals were anesthetized with a 3% isoflurane/O_2 gas mixture and maintained with a 1–1.5% isoflurane/O_2 gas mixture delivered through a nose cone. The mice were placed in a 30-mm birdcage coil with an animal handling system. A respiratory pillow was placed under the abdomen and ECG probes on the left forepaw and right hindpaw were used to monitor the heartrate and respiration rate. The aortic arch with all three branches (the brachiocephalic trunk, left common carotid artery, and left subclavian artery) were identified in a longitudinal position. MRI was performed using a T_1-weighted cardiac sequence. A 1 mm thick slice was acquired using a flash sequence. The repetition time and echo time for the T_1-weighted images were 10 ms and 3 ms, respectively. One signal average was used with a total imaging time of about 3 minutes per scan. For the experiment, ApoE KO mice fed on a high-fat diet for 4 months were first subject to a baseline scan and then administered with Gd-PNPs intravenously *via* the tail vein at a dose of 16 μmol Gd/kg.[43] Postcontrast MRI was done after 1 hour using the same parameters as the baseline scan.

Author Manuscript Author Manuscript Author Manuscript Author Manuscript

After the live imaging, the mice were euthanized and the aortic arch was collected for Oil Red O staining to confirm the presence of plaque.

Acknowledgments

This work is supported by the National Institutes of Health under Award Number R01CA200574 and the National Science Foundation Grant DMR-1505699. We thank Christopher V. Barback for his help with the MRI imaging.

References

1. Townsend N, Wilson L, Bhatnagar P, Wickramasinghe K, Rayner M, Nichols M. Cardiovascular Disease in Europe: Epidemiological Update 2016. Eur Heart J. 2016; 37:3232–3245. [PubMed: 27523477]
2. Roth GA, Huffman MD, Moran AE, Feigin V, Mensah GA, Naghavi M, Murray CJ. Global and Regional Patterns in Cardiovascular Mortality from 1990 to 2013. Circulation. 2015; 132:1667–1678. [PubMed: 26503749]
3. Ross R. The Pathogenesis of Atherosclerosis — An Update. N Engl J Med. 1986; 314:488–500. [PubMed: 3511384]
4. Tabas I, Garcia-Cardena G, Owens GK. Recent Insights into the Cellular Biology of Atherosclerosis. J Cell Biol. 2015; 209:13–22. [PubMed: 25869663]
5. Parthasarathy S, Steinberg D, Witztum JL. The Role of Oxidized Low-Density Lipoproteins in the Pathogenesis of Atherosclerosis. Annu Rev Med. 1992; 43:219–225. [PubMed: 1580586]
6. Stocker R, Keaney JF Jr. Role of Oxidative Modifications in Atherosclerosis. Physiol Rev. 2004; 84:1381–1478. [PubMed: 15383655]
7. Moore KJ, Sheedy FJ, Fisher EA. Macrophages in Atherosclerosis: A Dynamic Balance. Nat Rev Immunol. 2013; 13:709–721. [PubMed: 23995626]
8. Tabas I. Macrophage Death and Defective Inflammation Resolution in Atherosclerosis. Nat Rev Immunol. 2010; 10:36–46. [PubMed: 19960040]
9. Hansson GK, Libby P. The Immune Response in Atherosclerosis: A Double-Edged Sword. Nat Rev Immunol. 2006; 6:508–519. [PubMed: 16778830]
10. McCullagh KG, Duance VC, Bishop KA. The Distribution of Collagen Types I, III and V (AB) in Normal and Atherosclerotic Human Aorta. J Pathol. 1980; 130:45–55. [PubMed: 6991657]
11. Shekhonin BV, Domogatsky SP, Muzykantov VR, Idelson GL, Rukosuev VS. Distribution of Type I, III, IV and V Collagen in Normal and Atherosclerotic Human Arterial Wall: Immunomorphological Characteristics. Coll Relat Res. 1985; 5:355–368. [PubMed: 3902343]
12. Fox K, Garcia MA, Ardissino D, Buszman P, Camici PG, Crea F, Daly C, De Backer G, Hjemdahl P, Lopez-Sendon J, Marco J, Morais J, Pepper J, Sechtem U, Simoons M, Thygesen K. Guidelines on the Management of Stable Angina Pectoris: Executive Summary. Eur Heart J. 2006; 27:1341–1381. [PubMed: 16735367]
13. Fuster V, Stein B, Ambrose JA, Badimon L, Badimon JJ, Chesebro JH. Atherosclerotic Plaque Rupture and Thrombosis. Evolving Concepts. Circulation. 1990; 82:II47–59. [PubMed: 2203564]
14. Lutgens E, van Suylen RJ, Faber BC, Gijbels MJ, Eurlings PM, Bijnens AP, Cleutjens KB, Heeneman S, Daemen MJ. Atherosclerotic Plaque Rupture: Local or Systemic Process? Arterioscler Thromb Vasc Biol. 2003; 23:2123–2130. [PubMed: 14512372]
15. Stampfer MJ, Hu FB, Manson JE, Rimm EB, Willett WC. Primary Prevention of Coronary Heart Disease in Women through Diet and Lifestyle. N Engl J Med. 2000; 343:16–22. [PubMed: 10882764]
16. Baber U, Mehran R, Sartori S, Schoos MM, Sillesen H, Muntendam P, Garcia MJ, Gregson J, Pocock S, Falk E, Fuster V. Prevalence, Impact, and Predictive Value of Detecting Subclinical Coronary and Carotid Atherosclerosis in Asymptomatic Adults: The BioImage Study. J Am Coll Cardiol. 2015; 65:1065–1074. [PubMed: 25790876]
17. Shah PK. Screening Asymptomatic Subjects for Subclinical Atherosclerosis: Can We, Does It Matter, and Should We? J Am Coll Cardiol. 2010; 56:98–105. [PubMed: 20620724]

Author Manuscript Author Manuscript Author Manuscript Author Manuscript

18. Dweck MR, Doris MK, Motwani M, Adamson PD, Slomka P, Dey D, Fayad ZA, Newby DE, Berman D. Imaging of Coronary Atherosclerosis — Evolution Towards New Treatment Strategies. Nat Rev Cardiol. 2016; 13:533–548. [PubMed: 27226154]
19. Joshi FR, Lindsay AC, Obaid DR, Falk E, Rudd JH. Non-Invasive Imaging of Atherosclerosis. Eur Heart J Cardiovasc Imaging. 2012; 13:205–218. [PubMed: 22277118]
20. Sandfort V, Lima JA, Bluemke DA. Noninvasive Imaging of Atherosclerotic Plaque Progression: Status of Coronary Computed Tomography Angiography. Circ Cardiovasc Imaging. 2015; 8:e003316. [PubMed: 26156016]
21. Packham MA, Mustard JF. The Role of Platelets in the Development and Complications of Atherosclerosis. Semin Hematol. 1986; 23:8–26. [PubMed: 3511536]
22. Huo Y, Ley KF. Role of Platelets in the Development of Atherosclerosis. Trends Cardiovasc Med. 2004; 14:18–22. [PubMed: 14720470]
23. Lievens D, von Hundelshausen P. Platelets in Atherosclerosis. Thromb Haemost. 2011; 106:827–838. [PubMed: 22012554]
24. Weber C. Platelets and Chemokines in Atherosclerosis: Partners in Crime. Circ Res. 2005; 96:612–616. [PubMed: 15802619]
25. Gawaz M, Langer H, May AE. Platelets in Inflammation and Atherogenesis. J Clin Invest. 2005; 115:3378–3384. [PubMed: 16322783]
26. Lindemann S, Kramer B, Seizer P, Gawaz M. Platelets, Inflammation and Atherosclerosis. J Thromb Haemost. 2007; 5(Suppl 1):203–211. [PubMed: 17635728]
27. Badimon L, Vilahur G. Thrombosis Formation on Atherosclerotic Lesions and Plaque Rupture. J Intern Med. 2014; 276:618–632. [PubMed: 25156650]
28. Badimon L, Padro T, Vilahur G. Atherosclerosis, Platelets and Thrombosis in Acute Ischaemic Heart Disease. Eur Heart J Acute Cardiovasc Care. 2012; 1:60–74. [PubMed: 24062891]
29. Hu CM, Fang RH, Wang KC, Luk BT, Thamphiwatana S, Dehaini D, Nguyen P, Angsantikul P, Wen CH, Kroll AV, Carpenter C, Ramesh M, Qu V, Patel SH, Zhu J, Shi W, Hofman FM, Chen TC, Gao W, Zhang K, et al. Nanoparticle Biointerfacing by Platelet Membrane Cloaking. Nature. 2015; 526:118–121. [PubMed: 26374997]
30. Fang RH, Hu CM, Luk BT, Gao W, Copp JA, Tai Y, O'Connor DE, Zhang L. Cancer Cell Membrane-Coated Nanoparticles for Anticancer Vaccination and Drug Delivery. Nano Lett. 2014; 14:2181–2188. [PubMed: 24673373]
31. Hu CM, Zhang L, Aryal S, Cheung C, Fang RH, Zhang L. Erythrocyte Membrane-Camouflaged Polymeric Nanoparticles as a Biomimetic Delivery Platform. Proc Natl Acad Sci US A. 2011; 108:10980–10985.
32. Pang Z, Hu CM, Fang RH, Luk BT, Gao W, Wang F, Chuluun E, Angsantikul P, Thamphiwatana S, Lu W, Jiang X, Zhang L. Detoxification of Organophosphate Poisoning Using Nanoparticle Bioscavengers. ACS Nano. 2015; 9:6450–6458. [PubMed: 26053868]
33. Bentzon JF, Otsuka F, Virmani R, Falk E. Mechanisms of Plaque Formation and Rupture. Circ Res. 2014; 114:1852–1866. [PubMed: 24902970]
34. Zhang L, Chan JM, Gu FX, Rhee JW, Wang AZ, Radovic-Moreno AF, Alexis F, Langer R, Farokhzad OC. Self-Assembled Lipid–Polymer Hybrid Nanoparticles: A Robust Drug Delivery Platform. ACS Nano. 2008; 2:1696–1702. [PubMed: 19206374]
35. Desideri G, Ferri C. Endothelial Activation. Sliding Door to Atherosclerosis. Curr Pharm Des. 2005; 11:2163–2175. [PubMed: 16026286]
36. Zadelaar S, Kleemann R, Verschuren L, de Vries-Van der Weij J, van der Hoorn J, Princen HM, Kooistra T. Mouse Models for Atherosclerosis and Pharmaceutical Modifiers. Arterioscler Thromb Vasc Biol. 2007; 27:1706–1721. [PubMed: 17541027]
37. Kotb S, Piraquive J, Lamberton F, Lux F, Verset M, Di Cataldo V, Contamin H, Tillement O, Canet-Soulas E, Sancey L. Safety Evaluation and Imaging Properties of Gadolinium-Based Nanoparticles in Nonhuman Primates. Sci Rep. 2016; 6:35053. [PubMed: 27725693]
38. Piao JG, Wang L, Gao F, You YZ, Xiong Y, Yang L. Erythrocyte Membrane is an Alternative Coating to Polyethylene Glycol for Prolonging the Circulation Lifetime of Gold Nanocages for Photothermal Therapy. ACS Nano. 2014; 8:10414–10425. [PubMed: 25286086]

Author Manuscript Author Manuscript Author Manuscript Author Manuscript

39. Zhu JY, Zheng DW, Zhang MK, Yu WY, Qiu WX, Hu JJ, Feng J, Zhang XZ. Preferential Cancer Cell Self-Recognition and Tumor Self-Targeting by Coating Nanoparticles with Homotypic Cancer Cell Membranes. Nano Lett. 2016; 16:5895–5901. [PubMed: 27513184]

40. Gao W, Fang RH, Thamphiwatana S, Luk BT, Li J, Angsantikul P, Zhang Q, Hu CM, Zhang L. Modulating Antibacterial Immunity *via* Bacterial Membrane-Coated Nanoparticles. Nano Lett. 2015; 15:1403–1409. [PubMed: 25615236]

41. Wei X, Gao J, Fang RH, Luk BT, Kroll AV, Dehaini D, Zhou JR, Kim HW, Gao WW, Lu WY, Zhang L. Nanoparticles Camouflaged in Platelet Membrane Coating as an Antibody Decoy for the Treatment of Immune Thrombocytopenia. Biomaterials. 2016; 111:116–123. [PubMed: 27728811]

42. Xu SW, Huang Y, Xie Y, Lan TA, Le K, Chen JW, Chen SR, Gao S, Xu XZ, Shen XY, Huang HQ, Liu PQ. Evaluation of Foam Cell Formation in Cultured Macrophages: An Improved Method with Oil Red O Staining and DiI-oxLDL Uptake. Cytotechnology. 2010; 62:473–481. [PubMed: 21076992]

43. Amirbekian V, Lipinski MJ, Briley-Saebo KC, Amirbekian S, Aguinaldo JGS, Weinreb DB, Vucic E, Frias JC, Hyafil F, Mani V, Fisher EA, Fayad ZA. Detecting and Assessing Macrophages *In Vivo* to Evaluate Atherosclerosis Noninvasively using Molecular MRI. Proc Natl Acad Sci US A. 2007; 104:961–966.

Author Manuscript Author Manuscript Author Manuscript Author Manuscript

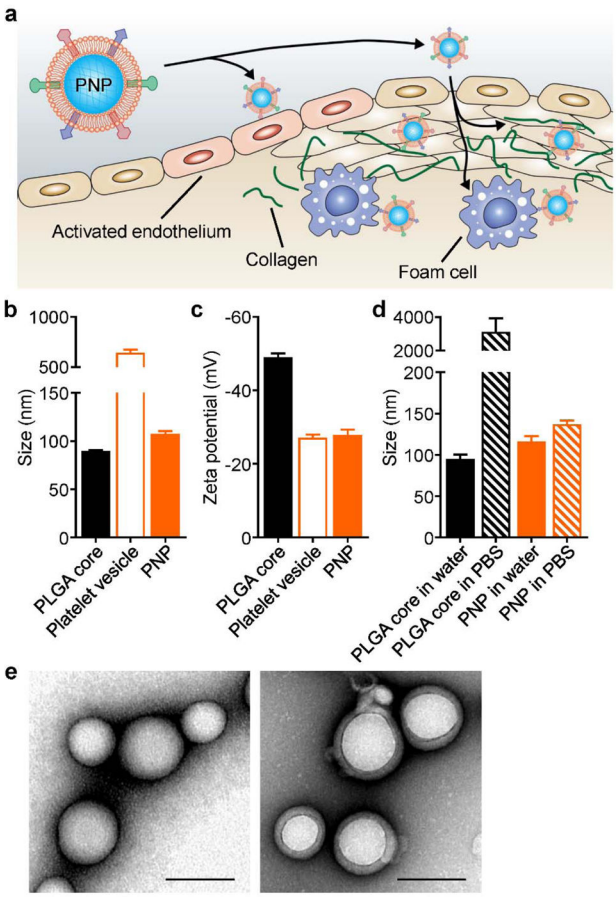

Figure 1.

Platelet membrane-coated nanoparticle (PNP) schematic and characterization. (a) PNPs express a variety of surface markers capable of targeting different components of atherosclerotic plaques, including activated endothelium, foam cells, and collagen. (b) Z-average size of bare PLGA cores, platelet membrane-derived vesicles, and PNPs as measured by dynamic light scattering (DLS) (n = 3, mean ± SD). (c) Surface zeta potential of bare PLGA cores, platelet membrane-derived vesicles, and PNPs as measured by DLS (n = 3, mean ± SD). (d) Z-average size of bare PLGA cores and PNPs in water or in PBS (n = 3, mean ± SD). (e) Transmission electron microscopy (TEM) image of bare PLGA cores (left) and PNPs (right) negatively stained with uranyl acetate (scale bars = 100 nm).

Author Manuscript Author Manuscript Author Manuscript Author Manuscript

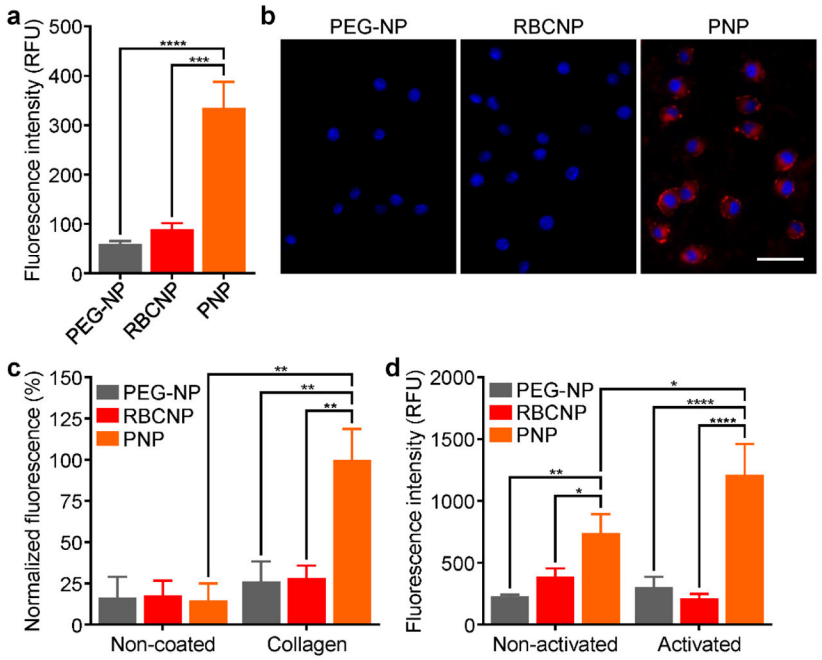

Figure 2.

In vitro targeting. (a,b) Binding of PEG-NPs, RBCNPs, or PNPs to foam cells as demonstrated by (a) flow cytometry (n = 3, mean ± SD) and (b) fluorescence microscopy (blue = nuclei, red = nanoparticle; scale bar = 50 μm). (c) Fluorescent quantification of PEG-NPs, RBCNPs, or PNPs bound to non-coated or collagen-coated surfaces (n = 3, mean ± SEM). (d) Fluorescent quantification of PEG-NPs, RBCNPs, or PNPs bound to HUVEC cells either in their normal state or after activation with tumor necrosis factor alpha (TNF-α) (n = 3, mean ± SD). *$p < 0.05$, **$p < 0.01$, ***$p < 0.001$, ****$p < 0.0001$; one-way ANOVA.

Author Manuscript Author Manuscript Author Manuscript Author Manuscript

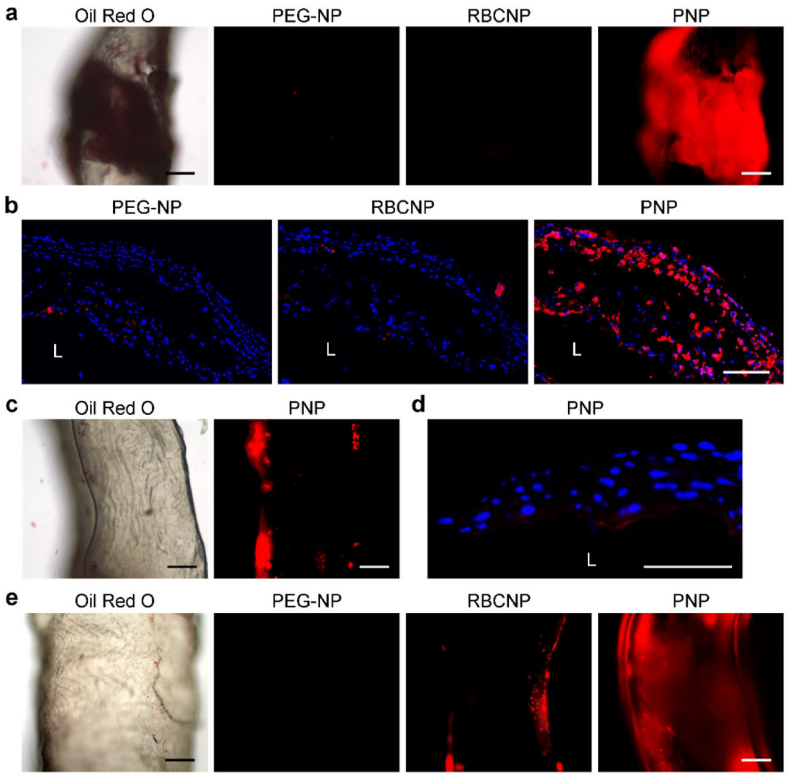

Figure 3.

Ex vivo binding to atherosclerotic plaque. (a) Binding of PEG-NPs, RBCNPs, or PNPs to part of an atherosclerotic aortic arch from ApoE knockout (KO) mice fed with a high fat western diet for 4 months (fluorescent images: red = nanoparticle; scale bar = 200 μm). Oil Red O staining was used to confirm the presence of plaque; the presented image is representative (bright field image: scale bar = 200 μm). (b) Fluorescent imaging of PEG-NPs, RBCNPs, or PNPs bound to histological cross-sections of atherosclerotic vessels of ApoE KO mice (L = luminal side; blue = nuclei, red = nanoparticle; scale bar = 100 μm). (c) Binding of PNPs to part of the aortic arch from a wild-type mouse (fluorescent image: red = nanoparticle; scale bar = 200 μm). Oil Red O staining was used to show the absence of plaque (bright field image: scale bar = 200 μm). (d) Fluorescent imaging of PNPs bound to a histological cross-section of a healthy vessel from a wild-type mouse (L = luminal side; blue = nuclei, red = nanoparticle; scale bar = 50 μm). (e) Binding of PEG-NPs, RBCNPs, or PNPs to a plaque-free region of the aortic arch from ApoE KO mice fed with a high-fat western diet (fluorescent images: red = nanoparticle; scale bar = 200 μm). Oil Red O staining was used to confirm the absence of plaque; the presented image is representative (bright field image: scale bar = 200 μm).

Author Manuscript Author Manuscript Author Manuscript Author Manuscript

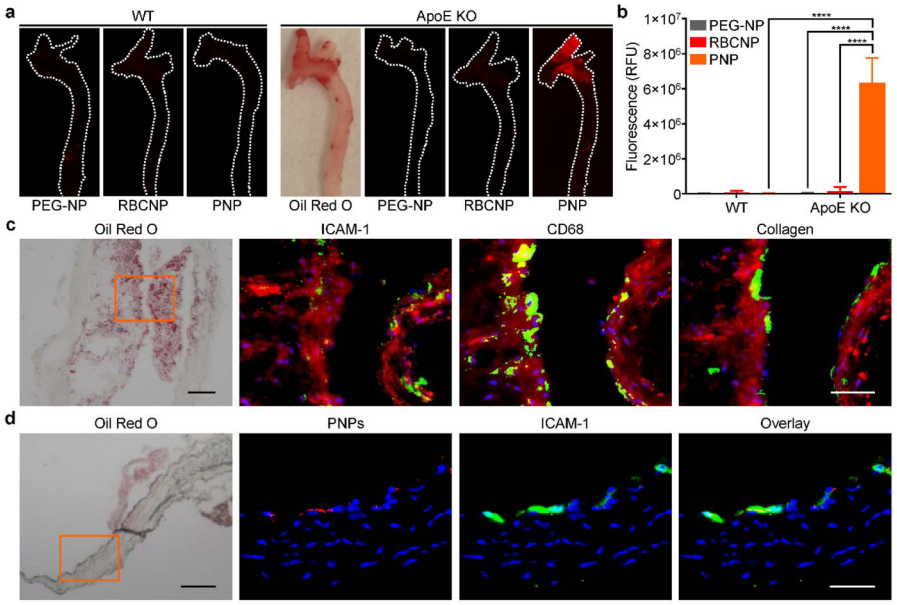

Figure 4.

In vivo targeting of atherosclerotic plaque. (a) Macroscopic fluorescent imaging of aortic arches from wild-type (WT) or ApoE KO mice fed on a high fat western diet after intravenous administration with PEG-NPs, RBCNPs, or PNPs (white = physical outline, red = nanoparticle). Oil Red O staining was used to confirm the presence of plaque for ApoE KO mice (image is representative). (b) Fluorescent quantification of the aortic arch of wild-type or ApoE KO mice after administration with PEG-NPs, RBCNPs, or PNPs (n = 3, mean ± SD). ****$p < 0.0001$; one-way ANOVA. (c) Histological cross-section of an aortic arch with significant atherosclerotic plaque from an ApoE KO mouse administered with PNPs. Slides were stained with antibodies against ICAM-1, CD68, or collagen (fluorescent images: blue = nuclei, red = nanoparticle, green = marker of interest, scale bar = 50 μm). Oil Red O staining indicates presence of atherosclerotic plaque (bright field image: orange box indicates region displayed in fluorescent images, scale bar = 100 μm). (d) Histological cross-section of an aortic arch with lesser developed atherosclerotic plaque from an ApoE KO mouse administered with PNPs. Slides were stained with an antibody against ICAM-1 (fluorescent images: blue = nuclei, red = nanoparticle, green = marker of interest, scale bar = 50 μm). Oil Red O staining indicates presence of atherosclerotic plaque (bright field image: orange box indicates region displayed in fluorescent images, scale bar = 100 μm).

Author Manuscript Author Manuscript Author Manuscript Author Manuscript

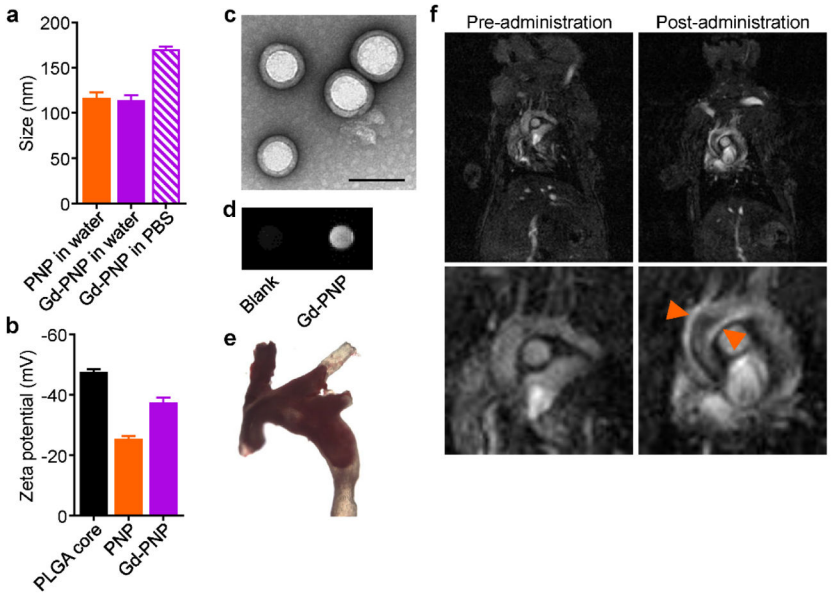

Figure 5.

Live imaging of atherosclerotic plaque. (a) Z-average size of PNPs and PNPs incorporated with Gd-chelated lipids as a contrast agent, termed Gd-PNPs, in water or in PBS as measured by DLS (n = 3, mean ± SD). (b) Surface zeta potential of bare PLGA cores, PNPs, and Gd-PNPs as measured by DLS (n = 3, mean ± SD). (c) TEM image of Gd-PNPs negatively stained with uranyl acetate (scale bar = 100 nm). (d) T_1-weighted signal of Gd-PNPs was confirmed by MRI. (e) Bright field image of aortic arch from ApoE KO mice stained with Oil Red O confirmed the presence of atherosclerotic plaque. (f) T_1-weighted MRI images of ApoE KO mice before and 1 hour after administration with Gd-PNPs (orange arrows = regions of positive contrast along aortic arch).